

INSTABILITIES IN FLOWS THROUGH CURVED DUCTS

Joana M.Malheiro^{1*}, Paulo J.Oliveira¹ and Fernando T.Pinho²

1: Unit of Textile and Paper Materials
Department of Electromechanical Engineering - Faculty of Engineering
University of Beira Interior
Calçada Fonte do Lameiro, 6200-001 Covilhã, Covilhã, Portugal
*e-mail: joanamouramalheiro@gmail.com web: <http://webx.ubi.pt/~mtp/>

2: Transport Phenomena Research Centre - CEFT
Faculty of Engineering – Department of Chemical Engineering
University of Porto
Rua Dr.Roberto Frias s/n, 4200-465 Porto, Porto, Portugal
web: <http://paginas.fe.up.pt/~ceft/Welcome.html>

Keywords: curved ducts, square cross-section, numerical methods, secondary flow, Newtonian fluid, viscoelastic fluid

Abstract *It is well known that flows in curved ducts give rise to an instability that manifests itself as the formation of secondary flow patterns (cells in the transversal plane, perpendicular to the main flow direction). The mechanism for this behaviour was explained by Dean back in the 1930th and it is basically due to an in-balance between centrifugal forces and the radial pressure gradient, tending to occur at moderate Reynolds number and therefore being a kind of inertia-generated instability. Later, in the 1970's, a new pair of cells was observed by Cheng and Akiyama for Reynolds numbers beyond a certain critical value, thus highlighting the complexity of flows with curvature, even with Newtonian fluids. When the fluid is non-Newtonian and exhibits viscoelastic characteristics, the same kind of secondary flow patterns is generated at much lower Reynolds number and the instability becomes controlled by elastic effects instead of inertial ones. In this work we give preliminary results for the Newtonian flow instability at Reynolds number of order 600, in which case comparison against existing results by others gives an indication of the correctness of our simulations, and for the non-Newtonian viscoelastic flow instability that occurs at a certain level of elasticity, at different Reynolds number.*

1. INTRODUCTION

The industrial and engineering applications of curved channels are many and of great interest. This interest comes from the centrifugal induced secondary flows, first reported by Eustice in 1911 and analytically confirmed by Dean in 1927, which is observed only in curved channels. The advantage of using curved channels is due to the effects produced by the secondary flow, examples are the improvement of heat and mass transfer coefficient, the increasing cross-sectional mixing and residence time of the fluid particles, among others [1][2]. In addition, the flow shows to be much more stable, the critical Reynolds number (Re) larger and the flux through the channel smaller than that in a straight duct. [1][3]

The secondary flow in curved channels is induced by unbalanced forces resulting in a pressure gradient across the channel cross-section. Thus, the secondary flow consists of a crosswise flow of slower-moving fluid near the walls (where viscosity forces are important and centrifugal forces are small, and because no-slip condition has to be satisfied) from the outerwall to the innerwall and the flow in the centre, of faster-moving fluid, from the inside to the outside of the bend (where viscosity forces have no influence and centrifugal forces are important, and because continuity must be respected). Transporting, this way, fluid from the outerwall to the innerwall along the walls and from the innerwall to the outerwall through the core.

The flow in curved channels is characterized by two symmetrical vortices that occupy the entire cross-section of the channel and its magnitude is measured by the Dean number (Dn). The Dean number is defined by the ratio of the inertial and centrifugal forces to the viscous force [4]:

$$Dn = \frac{Re}{\sqrt{Rc}} \quad (1)$$

where $Re = \frac{\rho U a}{\mu}$ is the Reynolds number and $Rc = \frac{R}{a}$ is the curvature ratio. U is the average velocity at inlet, a is the side of the square cross section and R is the radius of curvature of the channel. Although the secondary flow is characterized by a pair of vortices, as Re is increased, in the laminar regime, a second symmetrical pair of counter-rotating vortices appears near the outer wall [4]. Bara *et al* [4] described well and with some detail this phenomena, in curved channels with square cross-section. The appearance of this additional pair of vortices is not limited to a single value of Dn . Instead, it can appear in a range of Dn values where two solutions (one with one pair of vortices and other with two pairs of vortices, first reported by Cheng and Akiyama [5], in 1970) can be observed depending on the assumed conditions. In a numerical and experimental study of a curved duct with semicircular cross-section of flat outer wall, Masliyah [6] indicated the critical Dn number (above which four-vortex flow occurs) as 105. However, depending on the initial value of the flow field the numerical solution converges to either a two or four symmetric vortex flow, and two different solutions are possible for $Dn > 105$. Later, Winters [7] presented the numerical solution of a fully developed flow in a curved square

channel as a complex bifurcation diagram with regions of numerous solutions containing symmetric and asymmetric flows. Soh [10] also verified the existence of dual solutions and presented different critical Dn numbers for each case studied.

Although the appearance of an additional pair of vortices is already proved in curved square channels, the value at which the transition of two-vortices flow into four-vortices flow occurs and whereas the four-vortices flow is stable or not, are not yet in agreement. The different kind of methods used (numerical and experimental), the parameters considered (curved ratio, length of the channel, inlet conditions, cross-section geometry etc.) are among the reasons why no agreement is reached. Sugiyama *et al* [9], by flow visualization, described the development of the secondary flow and confirm the appearance of an additional pair. They considered different aspect ratio and curvature ratios, and show the relation between these two parameters and the critical Dn number, for the parameters they considered.

Later, Mees *et al* [8], by numerical simulating a fluid flow through a curved channel with square cross-section, showed that at $Dn = 453$ a third pair of highly unstable counter-rotating vortices appears near the outerwall side by side to the additional pair of vortices. And more recently, Helin *et al* [11], following the same geometry of Bara *et al* [4], presented results of the development of the flow considering a viscoelastic fluid. Using a Phan-Thien-Tanner (PTT) fluid, they found out that: the transition to the two-pair of vortices secondary flow appears earlier in the curve as inertia is increased and is delayed as the power-law index n of the PTT model is increased and as the extensional parameter of the fluid model is decreased. By considering an Oldroyd-B fluid, they also showed that the magnitude and intensity of the secondary vortices increase with elasticity.

The present research work is an extension of former works on Dean flows in curved channel with square cross-section, and is considered the same problem as Bara *et al* [4] and, later, Mees *et al* [8] and Helin *et al* [11]. However, here will be considered Newtonian and FENE-CR fluid model for a wide range of Reynolds and Deborah numbers.

2. GOVERNIG EQUATIONS

In this work was considered three-dimensional, laminar, isothermal, steady flow of an incompressible fluid. Two different fluid models were used: Newtonian and the viscoelastic fluid model FENE-CR. The conservation equations of mass and momentum in the absence of body forces, are presented below respectively:

$$\nabla \cdot \mathbf{u} = 0 \quad (2)$$

$$\rho \frac{D\mathbf{u}}{Dt} \equiv \rho \frac{\partial \mathbf{u}}{\partial t} + \rho \mathbf{u} \cdot \nabla \mathbf{u} = -\nabla p + \nabla \cdot \boldsymbol{\tau}_{tot} \quad (3)$$

where \mathbf{u} is the velocity vector (with u , v and w components for the x , y and z directions, respectively), ρ is the fluid density, t is the time, p the pressure and $\boldsymbol{\tau}_{tot}$ the extra stress tensor. The extra stress tensor is defined as: $\boldsymbol{\tau}_{tot} = \boldsymbol{\tau}_s + \boldsymbol{\tau}$, where $\boldsymbol{\tau}_s$ is the contribution of the

solvent which follows the Newtonian constitutive equations:

$$\boldsymbol{\tau}_s = \eta_s \dot{\boldsymbol{\gamma}} = \eta_s \left(\nabla \mathbf{u} + (\nabla \mathbf{u})^T \right) = 2\eta_s \mathbf{D} \quad (4)$$

and $\boldsymbol{\tau}$ is the contribution of the polymer molecules to which is considered the FENE-CR model:

$$\boldsymbol{\tau} + \left(\frac{\frac{\nabla}{\lambda}}{f(\boldsymbol{\tau})} \boldsymbol{\tau} \right) = 2\eta_p \mathbf{D} \quad (5)$$

where $f(\boldsymbol{\tau})$ is the extensibility function and is written as:

$$f(\boldsymbol{\tau}) = \frac{L^2 + \left(\frac{\lambda}{\eta_p} \right) \text{tr}(\boldsymbol{\tau})}{L^2 - 3} \quad (6)$$

where the rate of strain tensor is $\mathbf{D} = \frac{1}{2}(\nabla \mathbf{u} + \nabla \mathbf{u}^T)$, η_s is the solvent viscosity, η_p is the polymer viscosity, λ the constant zero-shear rate relaxation time and L^2 the extensibility parameter.

The non-dimensional parameters considered here are:

$$\text{Dean number: } Dn = \frac{\text{Re}}{\sqrt{Rc}} \quad (7)$$

$$\text{Reynolds number: } \text{Re} = \frac{\rho U a}{\mu} \quad (8)$$

$$\text{Deborah number: } De = \frac{\lambda U}{a} \quad (9)$$

where U is the average velocity at inlet, a is the side of the square cross section and R is the radius of curvature of the channel $R = \frac{(R1 + R2)}{2}$, where $R1$ and $R2$ are the internal and the external radius of the curve, respectively.

3. NUMERICAL METHODOLOGY

3.1. Numerical Method

The governing equations are numerically solved with a finite-volume CFD code developed by Oliveira *et al* [12], based on a general non-orthogonal coordinate system and a collocated mesh arrangement. This method guarantees that mass and momentum are

conserved over the whole domain. In this method all variables (pressure, velocities and stresses) are calculated at the centre of each control volume (CV) and which are organized forming a computational mesh. The governing equations, already presented, are discretised by integration in space over CV and in time over time steps (when an unsteady flow is considered) using a fully implicit discretization, resulting in a system of linearized algebraic equations for the mass and momentum conservation, and constitutive equations. The resolution algorithm, which was applied as described in Oliveira *et al* [12] where a detailed description can be found, ensures the coupling of velocity and pressure fields, through iterative process of correcting pressure, so continuity is verified.

3.2. Geometry, Mesh and Boundary Conditions

In this paper, a three-dimensional Newtonian fluid flow through a curved channel with square cross-section is presented.

The dimensions of the channel used are the same as those of Bara *et al* [4], Mees *et al* [8] and Helin *et al* [11]. Thus, the channel is divided into three blocks (Figure 1.): a straight channel of width $a = 1$ and length $Le = 20a$ at the entrance; a connecting 180° curved channel, with internal radius $R1 = 14.6a$ and external radius $R2 = 15.6a$; and a straight channel at the exit, having the same dimensions as the inlet channel. The aspect ratio k , which is defined by the height of the duct a divided by width of the duct a , is $k = 1$

(square cross-section), the radius of curvature is $R = 15.1$ and the curvature ratio $Rc = \frac{R}{a}$ is also 15.1.

The origin of the Cartesian coordinates system is at the bottom corner of the first block (Figure 1.) and the channel has a computational domain between $x = [0, 35.6]$, $y = [0, 31.2]$ and $z = [0, 1]$.

A non-uniform spaced mesh has been used and its geometrical characteristics are presented in Table 1. In this table is showed the number of cells in each block (N_x in direction x , N_y in direction y and N_z in direction z), the total number of control volumes (NCV) and the factor of compression/expansion (f_x , where $x = x, y$ or z depending on the direction considered). The mesh consists of: 224 nodes in the streamwise direction (31 nodes located in each straight part of the channel, non-uniformly distributed, and the rest uniformly spaced in the curved), 21 nodes in the normal direction and 21 nodes in the spanwise direction, both uniformly spaced. The size of consecutive cells varies with the factor of compression/expansion, defined by $\Delta x_{i+1} = f_x \Delta x_i$ where $x = x, y$ or z and Δx_i is the size of the cell i in a certain direction. The value of this factor is such that guarantee smooth transition in cells dimensions. Thus, in Block II and, Block I and III in y and z direction, the mesh is uniform so it takes the value of one. In Blocks I and III the mesh is non-uniform in x direction, and the compression factor is about 4.8% and the expansion factor is about 5%, respectively.

A no-slip condition is applied at the walls ($u = v = w = 0$), which are considered rigid. A fully developed velocity profile is imposed at the inlet of the entrance channel, in order to guarantee that the flow is fully developed when entering the curved part of the channel. At

the exit of the outlet channel a zero axial-gradient condition was imposed. The simulations were done using the entire domain of the channel, due to the possibility of occurrence of asymmetries in the flow [7]. The properties of the fluid are considered constant.

	Mesh			
	$N_x \times N_y \times N_z$	f_x	f_y	f_z
Block I	$30 \times 20 \times 20$	0.95212	1.00000	1.00000
Block II	$161 \times 20 \times 20$	1.00000	1.00000	1.00000
Block III	$30 \times 20 \times 20$	1.05029	1.00000	1.00000
NCV	88400			

Table 1. Geometrical characteristics of the computational mesh.

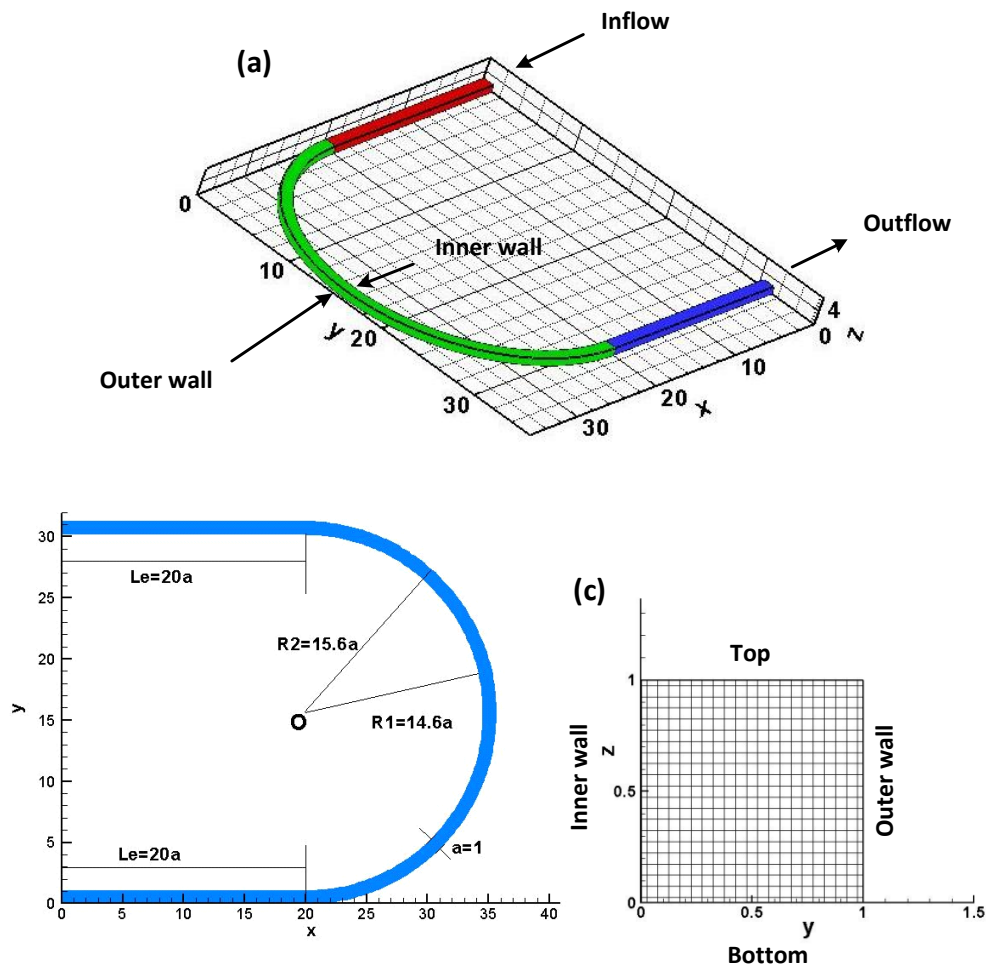


Figure 1. Geometry and mesh: a) general view of the channel with blocks represented by different colours; b) section of the plane z of the channel and c) cross-section of the channel with mesh.

4. RESULTS AND DISCUSSION

The results here presented are divided into two major groups: Newtonian and viscoelastic fluids. For both, plots of velocity profiles, contours and velocity fields are showed.

Taking into account Newtonian fluids, velocity profiles are shown for a wide range of values of Re ($1 \leq Re \leq 600$) and are compared with Bara *et al* [4] velocity profiles for $Re = 486, 532$ and 583 . The velocity fields are plotted only at two different angles (90° and 180°) also for various values of Re .

On the other hand, for viscoelastic fluids, velocity profiles are presented for a smaller range of Reynolds number and only for small values of Deborah number ($De \leq 0.5$). The velocity fields are also plotted at $\theta = 90^\circ$ and 180° .

4.1. Newtonian

Before proceeding to the velocity profiles, Figures 2 and 3 show the contours of dimensionless axial velocity for $Re = 1$ and 100 , respectively. In Figure 2., it can be seen that maximum velocity stays in the centre of the channel along the curve. At this Re the centrifugal forces are not strong enough to overcome viscous forces and the velocity remains unchangeable along the 180° curve.

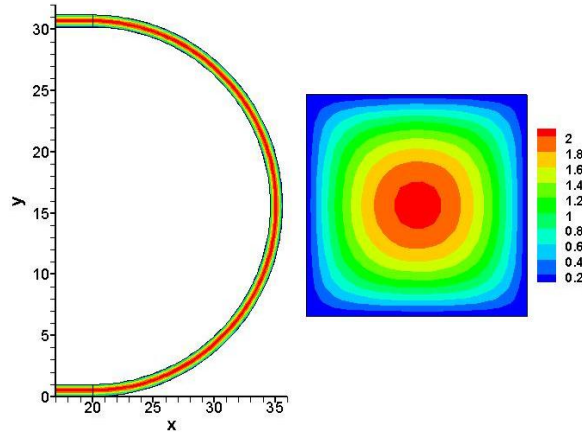


Figure 2. Contours of dimensionless axial velocity of the central plane, $z = 0.5$ (left) and cross-section (right), for $Re = 1$.

However, as the Re is increased, centrifugal forces get stronger, overcoming viscous forces, and throws maximum velocity toward the outerwall of the curve. This happens just before $Re = 100$ and is showed in Figure 3. For $Re = 100$, at 0° maximum velocity is in the centre of the channel, due to fully developed inlet conditions, and forward in the channel ($\theta \approx 30^\circ$) moves toward the outerwall.

In order to guarantee that the inlet profiles used in the simulation were fully developed, the velocity profiles at different Re were compared with the velocity profile determined analytically, and Figure 4. reveal that the condition of fully developed flow inlet profile was assured during numerical simulations.

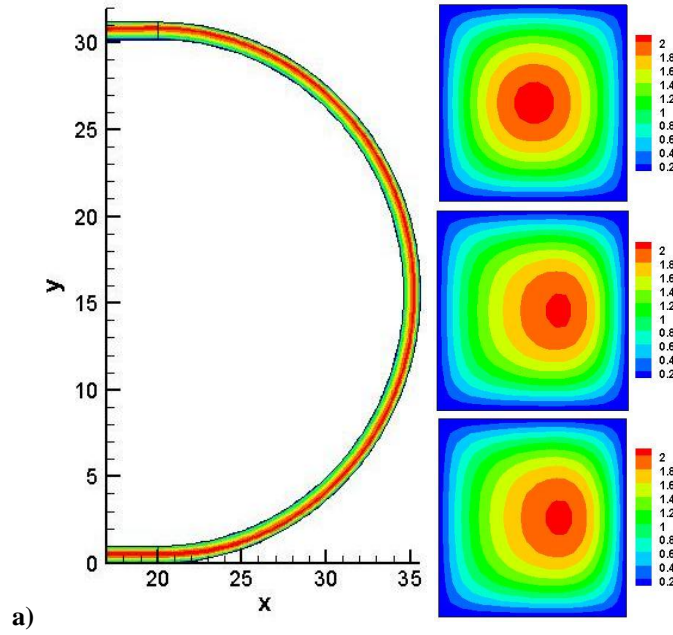


Figure 3. Contours of dimensionless axial velocity of the central plane, $z = 0.5$ (left) and cross-section (right) for $\theta = 0^\circ$, 90° and 180° (from top to bottom, respectively) for $Re = 100$.

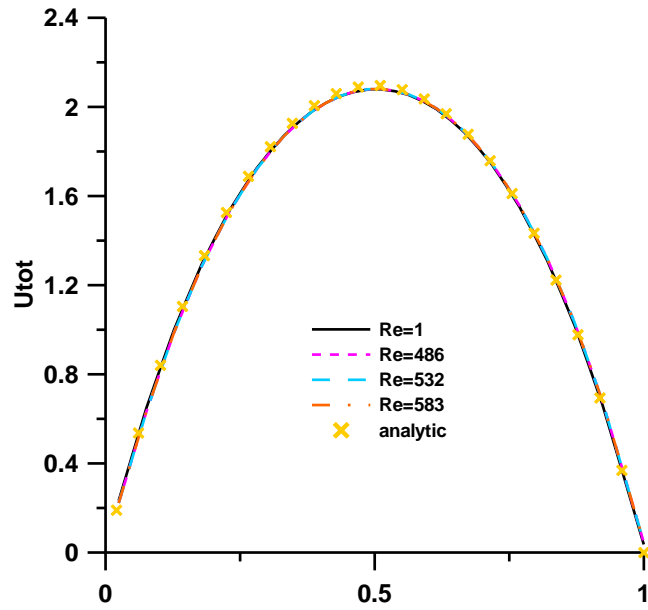


Figure 4. Velocity profiles at the inlet of the curve for different Re (1, 486, 532 and 483) and theoretically determined (analytic).

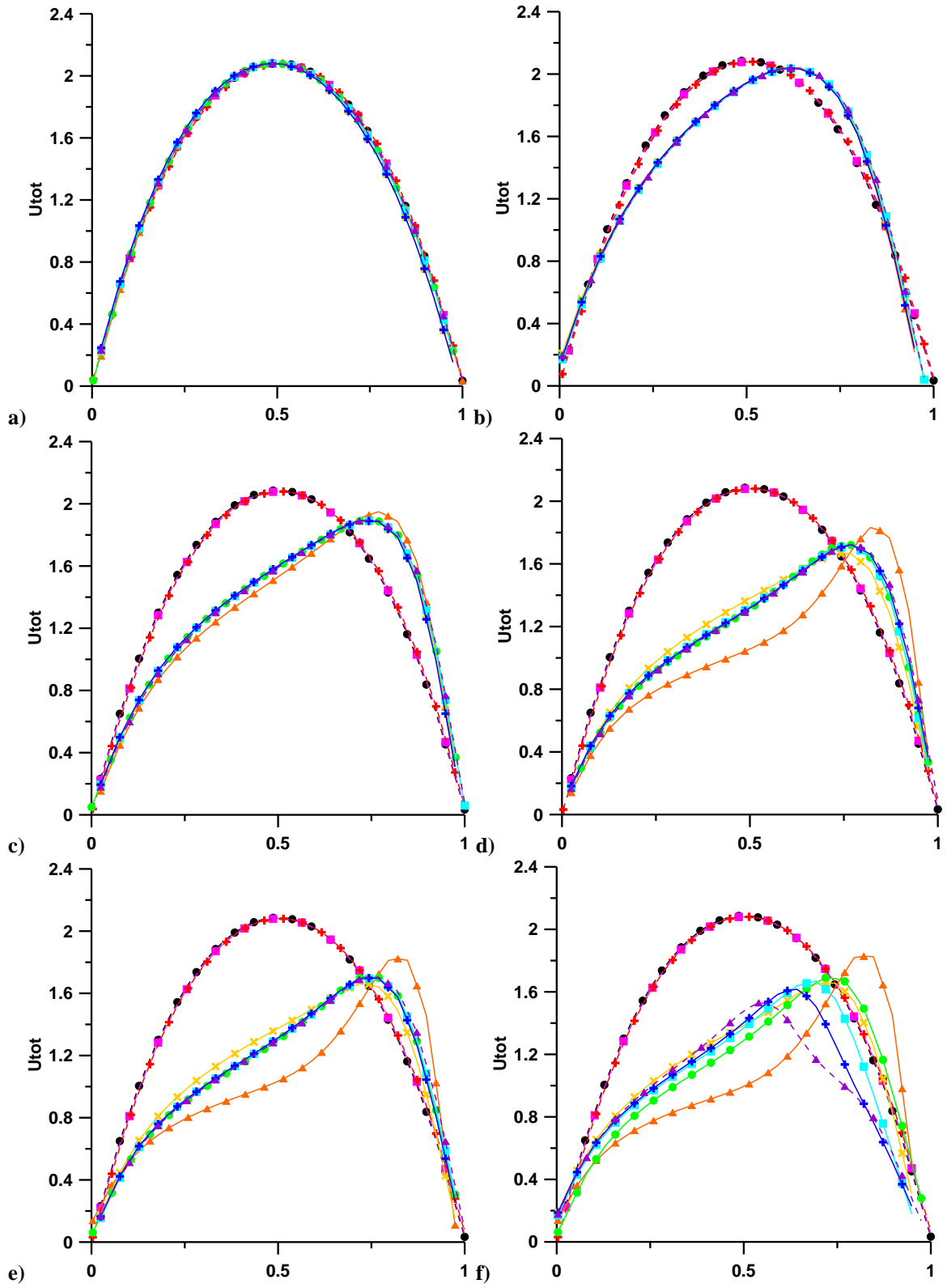
First, results of a Newtonian flow are presented. The set of velocity profiles in Figure 5. show the evolution of axial velocity along the 180° curved channel. The results of the

central plane, $z = 0.5$, for $Re = 1, 100, 200, 486, 532, 583$ and 600 are plotted for different angles ($\theta = 0^\circ, 30^\circ, 60^\circ, 90^\circ, 120^\circ, 150^\circ$ and 180°) of the curve and also for the entry and exit of the inlet straight channel.

For $Re = 1$ (Figure 5. a)), the velocity profile is parabolic along the length of the channel. Here the viscous forces are stronger than the centrifugal forces, causing maximum velocity to remain at the centre of the channel. As Re is increased (Figure 5. b)) centrifugal forces get stronger and start to overcome viscous forces, and slightly push maximum velocity toward the outerwall. This effect gets stronger as Re is increased from 100 to 200 (Figure 5. c)). Also in Figure 5. c), the velocity profile at $\theta = 30^\circ$ differs from the other profiles of the curved part of the channel by presenting a much higher magnitude and by being closer to the outerwall. This happens because when fluid enters into the curved part of the channel, coming from a straight channel and viscous forces have no effect, it flows as if still in a straight channel and runs against the outerwall of the channel. From this point on the maximum velocity slightly shifts towards the centre of the channel and its magnitude decreases. It can be also observed that for $Re = 200$ the curve length is sufficient so that flow reaches the fully development.

Increasing Re until 486 ($Dn = 125$) (Figure 5. d)) the behaviour exhibited by the flow for $Re = 200$ is verified, but this time with a higher intensity. In the beginning of the curve ($\theta = 30^\circ$) and due to inertia rising, the flow runs against the outerwall of the curve with higher velocity, presenting a higher peak. This initial transfer of momentum is a result of the fluid flowing through the curve following the line of the straight duct axis. However, the axial velocity near the innerwall decreases sharply. At 60° from the inlet, the peak in the velocity profile decrease and moves back toward the channel centre, and, also, the axial velocity near the innerwall increase. This redistribution of velocity is a result of the secondary flow transporting the high momentum fluid at the outerwall to the innerwall, filling in the central region of the velocity profile. At 90° there is a slight decrease in the axial velocity in the central region of the channel. After 90° no more appreciable changes are verified and the flow seems to become fully developed. In Figure 6. secondary flow is established and a symmetrical pair of counter rotating vortices, which occupy the cross-section of the channel, is formed.

The development of the axial velocity at different positions in the duct at $Re = 532$ ($Dn = 137$) is showed in Figure 5. e), and it can be seen that the development of the velocity profiles is very similar to the development at $Re = 486$. This result is contrary to that observed by Bara *et al* [4]. In their investigation, at $Dn = 137$, only up to $\theta = 80^\circ$ the axial velocity profiles present the same development as that of $Dn = 125$. They report that after $\theta = 80^\circ$ position, the flow development at $Re = 532$ starts to differ from that at $Re = 486$. While at $Re = 486$ the velocity profiles are already well established by $\theta = 100^\circ$, at $Re = 532$ the velocity profiles is slightly shifted back toward the channel centre. They justify this behaviour with the appearance of an additional pair of small counter rotating vortices near the outerwall, between 80° and 100° . They also report that the intensity of this additional pair of vortices grows with downstream distance, however, we did not identify any additional pair of vortices, either in the middle (Figure 7. a)) or at the end of the curve



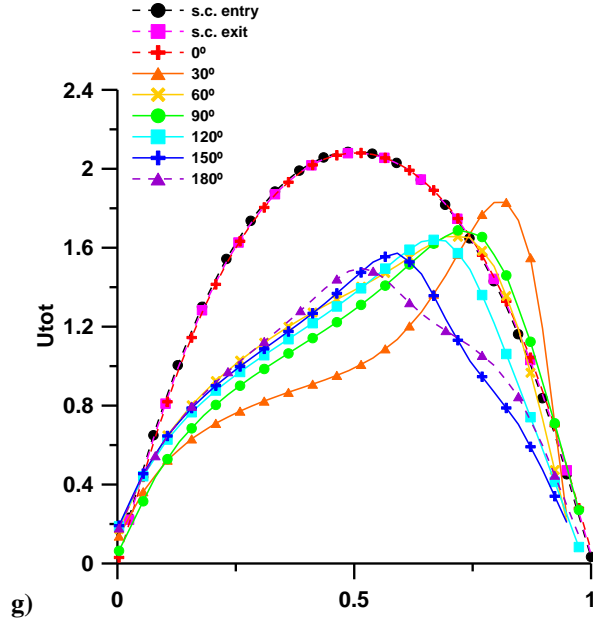


Figure 5. Velocity profiles at different values of θ along the curve for: a) $Re = 1$; b) $Re = 100$; c) $Re = 200$; d) $Re = 486$; e) $Re = 532$; f) $Re = 583$; g) $Re = 600$. NOTE: “s.c.” in the legend means “straight channel”.

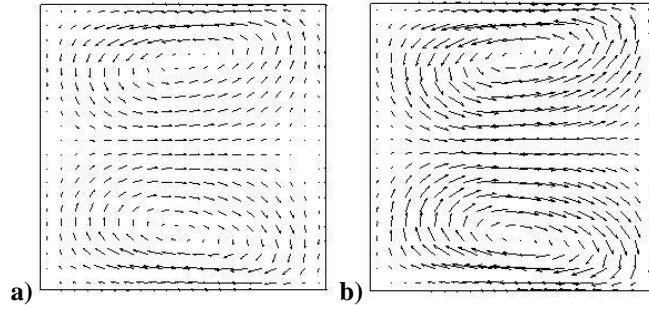


Figure 6. Velocity fields $Re = 486$ for a) 90° and b) 180° .

(Figure 7. b)). The curve used in the present study is only 180° long whereas in Bara *et al* [4] investigation the curve is 240° long. So, and despite the differences between both results for a 180° length, we cannot guarantee that our flow reached fully development and, as a consequence, we cannot guarantee that for a longer channel the additional pair of vortices may or may not appear.

The development of axial velocity with downstream position in the curved part of the duct at $Re = 583$ is shown in Figure 5. f). Up to $\theta = 60^\circ$ the flow development is practically the same at $Re = 583$ as it was at $Re = 486$ and 532 . At $\theta = 90^\circ$ the axial velocity profile starts to move back, transferring momentum toward the channel centre. This momentum transfer increase until the end of the curve, where the maximum velocity is located very close to the centre of the channel. This large momentum transfer is due to the development of an

additional pair of counter rotating vortices, which is verified in Figure 8. where the velocity fields at 90° and 180° are illustrated. Bara *et al* [4] reported that an additional pair of vortices starts to form, between $\theta = 80^\circ$ and $\theta = 100^\circ$, and we support that result with Figure 8. a), where an additional pair of vortices is identified at $\theta = 90^\circ$. Also, Bara *et al* [4] described an increase in the intensity of the additional pair of vortices in the downstream direction and their flow reached fully development. Similarly our result show an increase in intensity of the additional pair of vortices (Figure 8. b)) but fully developed flow was not reached.

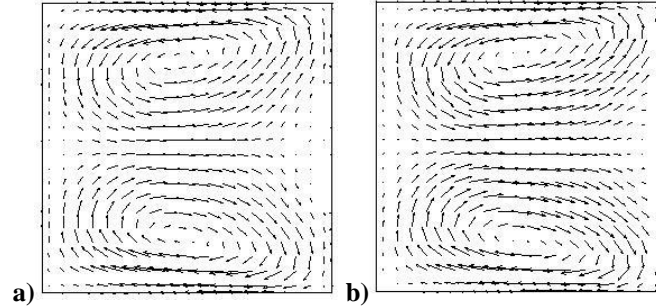


Figure 7. Velocity fields $Re = 532$ for a) 90° and b) 180° .

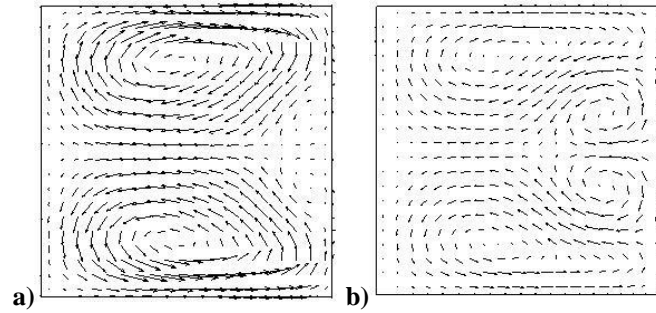


Figure 8. Velocity fields $Re = 583$ for a) 90° and b) 180° .

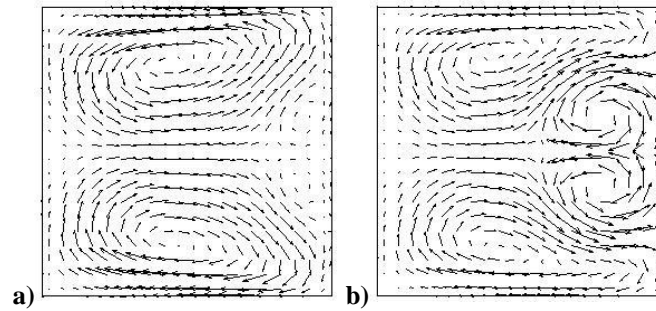


Figure 9. Velocity fields $Re = 600$ for a) 90° and b) 180° .

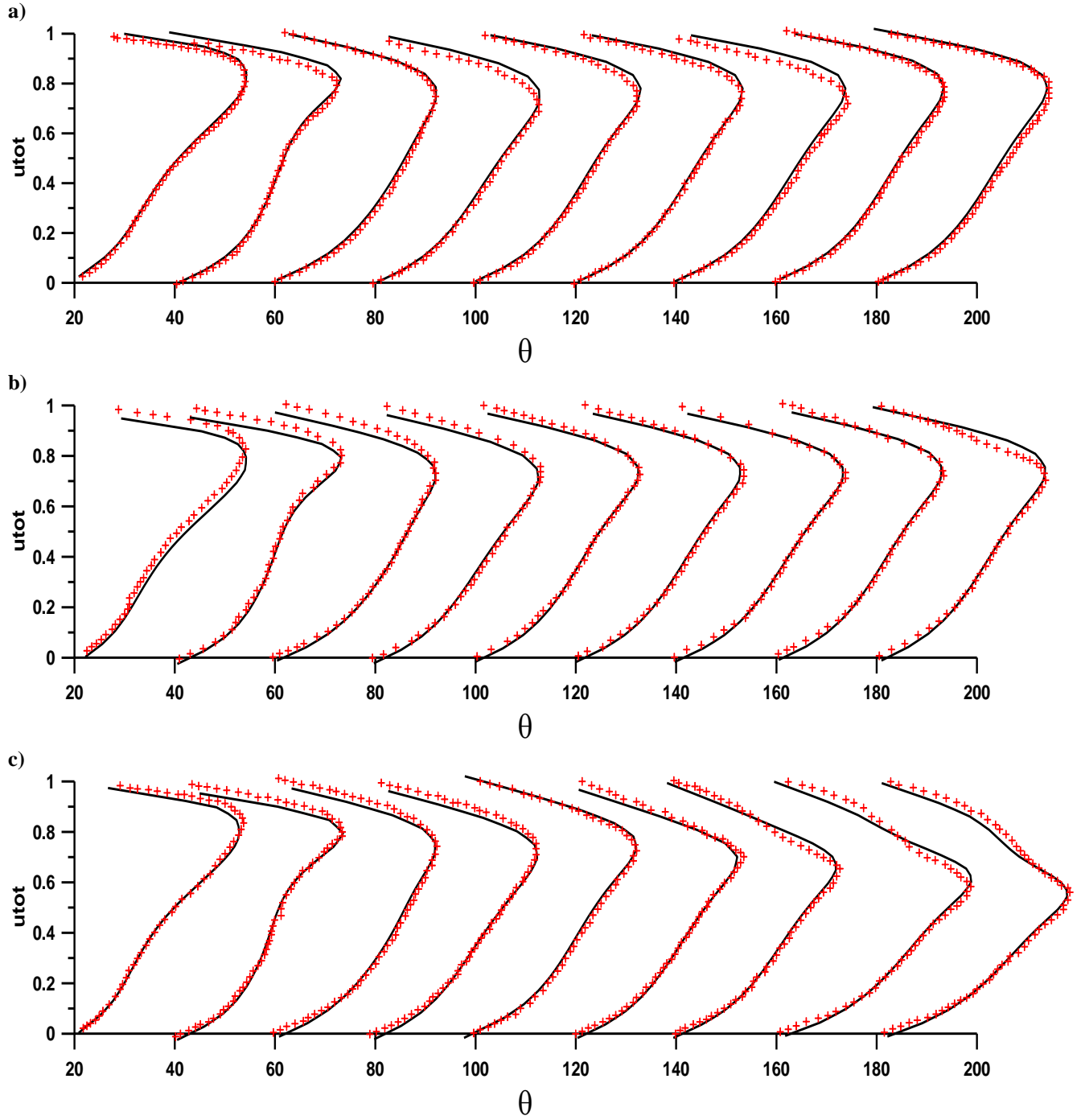


Figure 10. Comparison with Bara *et al* [4] results of the development of velocity profiles along the 180° curve: a) $Re = 486$ ($Dn = 125$); b) $Re = 532$ ($Dn=137$); c) $Re = 583$ ($Dn = 150$).

At $Re = 600$ (Figure 5. g)) the development of velocity profiles is very similar to that presented at $Re = 583$. In this case, the momentum transfer at the end of the channel (after $\theta = 150^\circ$) is higher and at $\theta = 180^\circ$ the maximum velocity is practically in the centre of the channel. Also the coming out of the additional pair of vortices is verified and with higher intensity, as it can be seen in Figure 9..

Figure 10. shows a comparison between the results that we obtained and those of Bara *et al* [4]. Although we have not recognize any significant movement of the momentum toward the centre of the duct or the appearance of the additional pair of counter rotating vortices after $\theta = 80^\circ$, when inertia is increased to $Re = 532$, is evident, by observing Figure 10., that good agreement was reached between our and Bara *et al* [4] results for all different Re numbers ($Re = 486, 532$ and 583).

4.2. Viscoelastic

To show the development of velocity profiles of viscoelastic fluid at different Deborah numbers (De), three Re were considered: 486, 532 and 583 and compared with the development of a Newtonian fluid velocity profile at the same Re . The results are only displayed at curve locations where results were relevant.

The first set of graphics (Figure 11.) illustrate the development of velocity profiles for increasing De up to 0.5 at $Re = 486$. The results are shown for the locations of $\theta = 90^\circ$ (middle of the curve) and 180° (end of the curve), and no differences are observed.

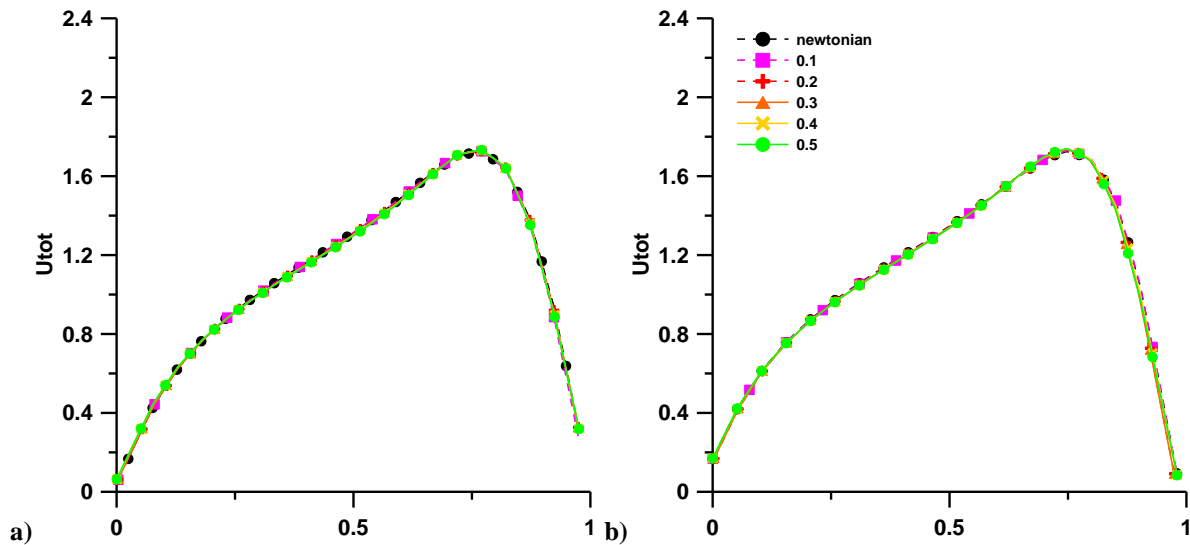


Figure 11. Development of velocity profiles of a Newtonian fluid and a viscoelastic fluid at different De ($0.1 \leq De \leq 0.5$) for $Re = 486$ at location a) 90° and b) 180° .

Increasing Re until 532 the influence of increasing De starts to be evident (Figure 12.). At $\theta = 150^\circ$, it can be seen, in Figure 12. b), that as De is increased the maximum of axial velocity slightly decrease in magnitude and it moves toward the centre of the channel. This behaviour is more prominent at the end of the curve (Figure 12. c)) where, at $De =$

0.5, the momentum transfer back to the centre of the channel is much higher than that of a Newtonian fluid. As a consequence of this growing momentum transfer with increasing De , an additional pair of counter rotating vortices is now observed at $Re = 532$ with $De = 0.5$ (Figure 13.). These results are in agreement with the conclusions reached by Helin *et al* [11], where the increased viscoelasticity of the fluid leads to an early onset of the additional pair of vortices.

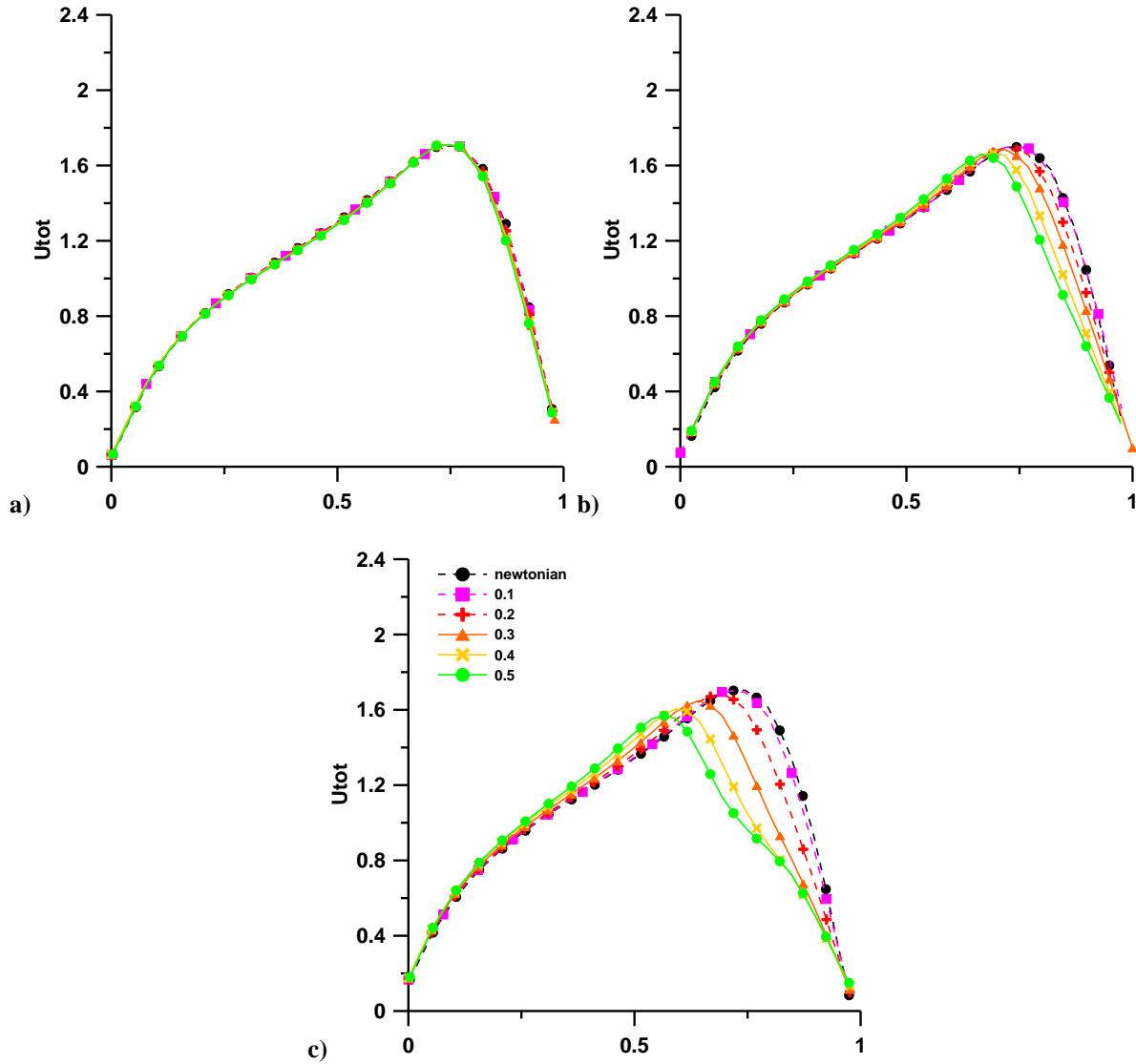


Figure 12. Development of velocity profiles of a Newtonian fluid and a viscoelastic fluid at different De ($0.1 \leq De \leq 0.5$) for $Re = 532$ at location a) 90° , b) 150° and c) 180°

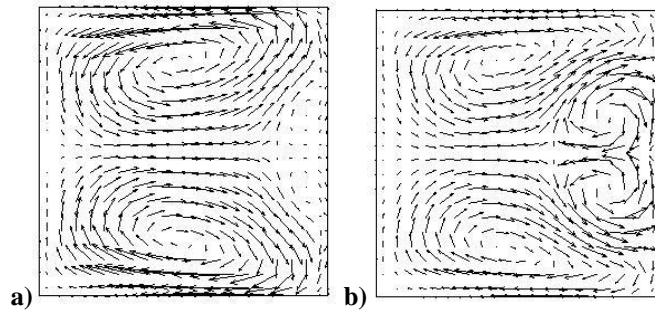


Figure 13. Velocity fields $Re = 532$ and $De = 0.5$ for a) 90° and b) 180° .

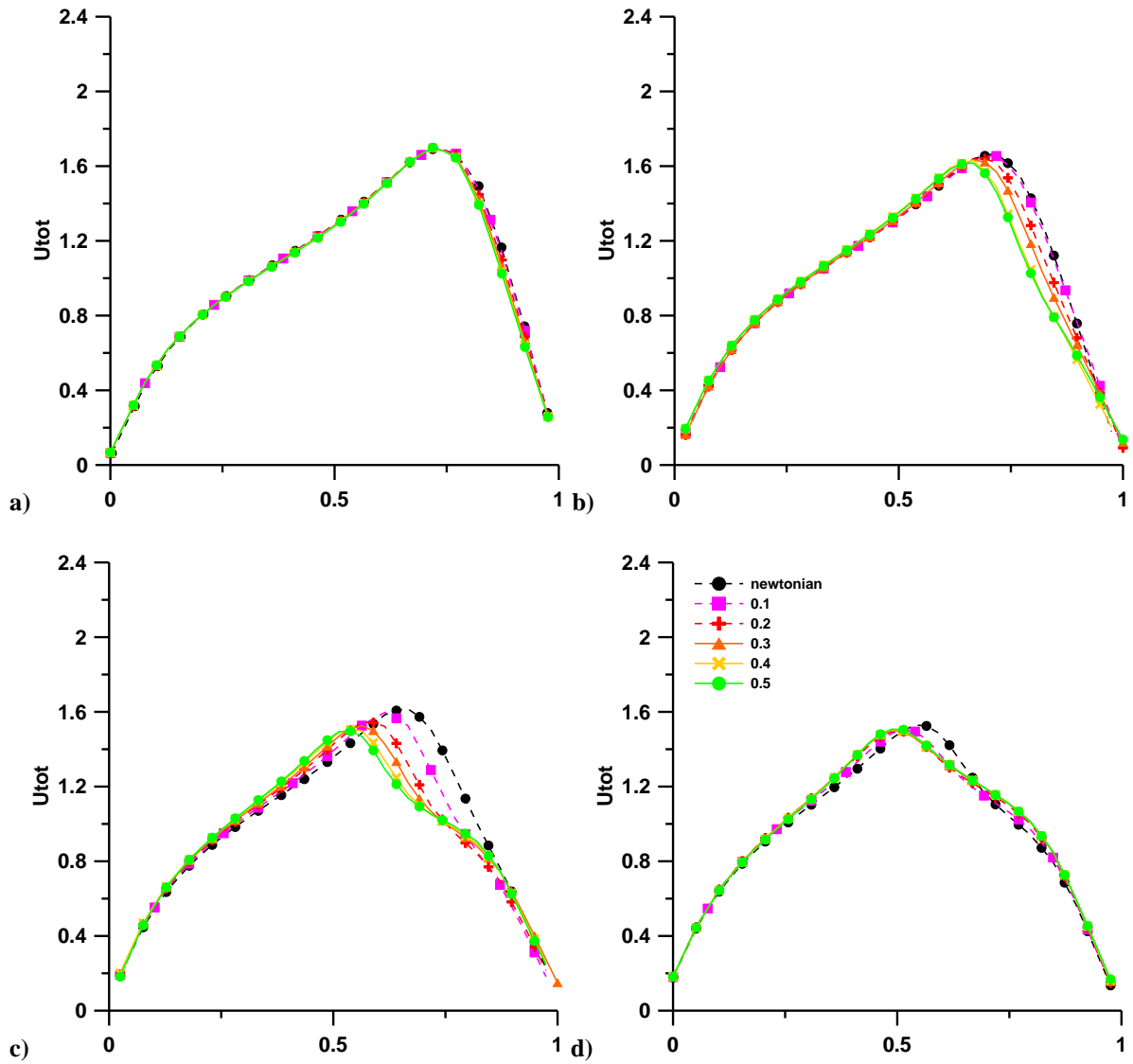


Figure 14. Development of velocity profiles of a Newtonian fluid and a viscoelastic fluid at different De ($0.1 \leq De \leq 0.5$) for $Re = 583$ at location a) 90° , b) 120° , c) 150° and d) 180° .

In Figure 14. and Figure 15. both velocity profiles and velocity fields are presented, respectively, at $Re = 583$ and for different De . By increasing inertia, the effects of De starts earlier in the channel. While at $Re = 532$ the effect of increasing De was significant only at $\theta = 150^\circ$ (Figure 12. b)), at $Re = 583$ this influence is verified at $\theta = 120^\circ$ (Figure 14. b)). In the same way as the last case, as De is increased a higher transfer of momentum to the centre of the duct is verified. The intensity of this transfer grows in the downstream direction until $\theta = 150^\circ$ (Figure 14. c)), after which location the effect of increasing De decrease sharply (Figure 14. d)). Comparing the velocity fields in Figure 13. and those at $Re = 583$ (Figure 15.), is clear that the additional pair of vortices at $Re = 583$ grow in intensity and size.

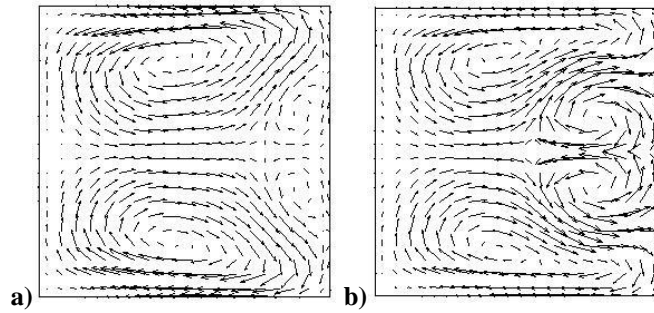


Figure 15. Velocity fields $Re = 583$ and $De = 0.5$ for a) 90° and b) 180° .

5. CONCLUSIONS

This numerical investigation was performed to verify the development of secondary flow for Newtonian and viscoelastic FENE-CR fluids. Numerical simulations were done for different Reynolds number ($Re \leq 600$), for both types of fluids and for different Deborah numbers ($De \leq 0.5$), for the viscoelastic fluid. The geometry of the channel chosen was the same as that used by different authors ([4], [8] and [11]) in order to better compare our results with those already published.

By comparing our results of a Newtonian fluid with those of Bara *et al* [4], we observed good agreement in all cases, when velocity profiles were analysed. However, looking to velocity fields, while Bara *et al* [4] reported the development of an additional pair of counter rotating vortices near the outerwall at $Re = 532$ and between $\theta = 80^\circ$ and 100° , we did not observed any additional pair of vortices even at the end of the curve (180°). Only at $Re = 583$, the onset of the additional pair of vortices was verified at location $\theta = 90^\circ$, and their intensity was higher at the end of the curve. The appearance of the additional pair of vortices is related to the transfer of momentum to the centre of the channel cross-section.

Regarding viscoelastic fluids, as De is increased the development of the secondary flow is no longer controlled by inertia, as it was in the case of Newtonian fluids. When De is increased from 0.1 to 0.5, the transfer of momentum grows and, the coming out of additional pair of vortices occurs earlier and with increasing intensity along the curve. Thus, while for the Newtonian fluid we found no trace of the additional pair of vortices at $Re = 532$, for the

viscoelastic fluid at $De = 0.5$ for the same Re are quite well developed.

REFERENCES

- [1] Berger, S.A., Talbot, L., Yao, L.-S., “Flow in Curved Pipes”, *Annual Review of Fluid Mechanics*, **15**, pp. 461-512, (1983).
- [2] Vashisth, S., Kumar, V., Nigam, K.D.P., “A Review on the Potential Applications of Curved Geometries in Process Industry”, *Industrial & Engineering Chemistry Research*, **47**, pp. 3291-3337, (2008).
- [3] Cuming, H.G., “The secondary flow in curved pipes”, *Aeronautical Research Council, Reports and Memoranda*, **2880**, (1952).
- [4] Bara, B., Nandakumar, K., Masliyah, J.H., “An experimental and numerical study of the Dean problem: flow development towards two-dimensional multiple solutions”, *Journal of Fluid Mechanics*, **244**, pp. 339-376, (1992).
- [5] Cheng, K.C., Akiyama, M., “Laminar forced convection heat transfer in curved rectangular channels”. *International Journal of Heat and Mass Transfer*, **13**, pp. 471-490, (1970).
- [6] Masliyah, J.H., “On laminar flow in curved semicircular ducts”, *Journal of Fluid Mechanics*, **99** (3), pp. 469-479, (1980).
- [7] Winters, K.H. “A bifurcation study of laminar flow in a curved tube of rectangular cross-section”. *Journal of Fluid Mechanics*, **180**, pp. 343-369, (1987).
- [8] Mees, P.A.J., Nandakumar, K., Masliyah, J.H., “Instability and transitions of flow in a curved square duct: the development of two pairs of Dean vortices”, *Journal of Fluid Mechanics*, **314**, pp. 227-246, (1996).
- [9] Sugiyama, S., Hayashi, T., Yamazaki, K., “Flow characteristics in the curved rectangular channels”, *Japan Society of Mechanical Engineers*, **26**(216), pp. 964-969, (1983).
- [10] Soh, W.Y., “Developing fluid flow in a curved duct of square cross-section and its fully developed dual solutions”, *Journal of Fluid Mechanics*, **188** pp. 337-361, (1988).
- [11] Helin, L., Thais, L., Mompean, G., “Numerical simulation of viscoelastic Dean vortices in a curved duct”, *Journal of Non-Newtonian Fluid Mechanics*, **156** pp. 84-94(2009).
- [12] P.J. Oliveira, F.T. Pinho and G.A. Pinto, “Numerical simulation of non-linear elastic flows with a general collocated finite-volume method”, *Journal of Non-Newtonian Fluid Mechanics*, **79**, pp. 1-43, (1998).